Journal of Sound and Vibration (2000) **233**(2), 279–295
doi:10.1006/jsvi.1999.2798, available online at http://www.idealibrary.com on IDEAL®

FORCING INDUCED ASYMMETRY ON DYNAMICAL SYSTEMS WITH CUBIC NON-LINEARITIES

G. VERROS AND S. NATSIAVAS

Department of Mechanical Engineering, Aristotle University, 54006 *Thessaloniki, Greece*

(*Received* 12 *July* 1999, *and in final form* 19 *November* 1999)

The present work investigates the dynamics of a class of two-degree-of-freedom oscillators with cubic non-linearity in the restoring forces. These oscillators are under the action of an external load including constant and harmonic components. Initially, a perturbation analysis is applied to the equations of motion, demonstrating the effect of the asymmetry induced by the constant loading component on the classical 1:1 and 1:3 internal resonances, as well as on the possibility of the appearance of a first order 1:2 internal resonance. Next, sets of slow-flow equations governing the amplitudes and phases of vibration are derived for the special case of no internal resonance and for the most complicated case corresponding to 1:1 internal resonance. The analytical findings are then complemented by numerical results, obtained by examining the dynamics of a two-degree-of-freedom mechanical system. First, the effect of certain system parameters on the existence and stability of constant and periodic solutions of the slow-flow equations is illustrated by presenting a sequence of response diagrams. Finally, the dynamics of the system used as an example is investigated further by direct integration of the slow-flow equations. This shows the existence of a period-doubling sequence culminating into a continual interchange between quasiperiodic and chaotic response. It also demonstrates a new transition scenario from phase-locked to phase-entrained and drift response.

1. INTRODUCTION

The response of mechanical systems with asymmetric stiffness and damping properties has been examined in a large number of previous investigations (e.g. references [1–5]). In particular, for multiple-degree-of-freedom dynamical systems with non-linear characteristics, one of the strongest effects is the appearance of a first order 1:2 internal resonance. On the other hand, non-linear systems with symmetric characteristics exhibit 1:1 and 1:3 resonances to first order [4–12]. Occasionally, they can also present asymmetric response due to symmetry-breaking bifurcations [10–13]. Moreover, besides the asymmetry in the constitutive properties, response asymmetry arises frequently in symmetric non-linear systems due to the presence of a constant component in the external loading [4].

The main objective of the present study is to investigate the effects of a load-induced asymmetry on the dynamics of a general class of mechanical systems with symmetric non-linearities in their restoring forces. More specifically, the dynamical systems examined are represented by a set of two coupled equations of motion. These equations are weakly non-linear and as a consequence, approximate analytical solutions can be obtained by applying suitable singular perturbation methodologies [4, 13]. Here the emphasis is placed on cases where conditions of primary external resonance are satisfied. Under such

0022-460X/00/220279 + 17 $35.00/0

conditions, different sets of slow-flow equations are derived for the amplitudes and phases of vibration arising in the case of no internal resonance and when 1 : 1 internal resonance is activated.

The dynamical system examined is presented in the following section in a quite general weakly non-linear form. Approximate analytical solutions are then obtained for the case of primary external resonance. Namely, sets of slow-flow equations are first derived for the amplitudes and phases of vibration by applying the method of multiple time scales. The simplest form of these equations appears in the case of no internal resonance. On the other hand, the most complex situation arises when conditions of 1 : 1 internal resonance are fulfilled. These cases are examined separately in sections 3 and 4 respectively. In section 5, an example of a mechanical system is introduced and its equations of motion are presented in the normalized form analyzed in the previous sections. Section 6 presents characteristic numerical results in the form of response diagrams, including constant and periodic solutions of the slow-flow equations. These results are accompanied with results obtained by direct integration of the slow-flow equations, demonstrating the existence of more complicated motions of the system, including a period-doubling sequence leading to chaos. They also illustrate a transition from phase-locked to phase-entrained and drift response. The final section summarizes the highlights of the study.

2. EQUATIONS OF MOTION — PERTURBATION ANALYSIS

The equations of motion for the class of dynamical systems examined in the study can be presented in the following normalized canonical form:

$$\ddot{u}_n + \omega_n^2 u_n + \varepsilon(\alpha_{n1}\dot{u}_1 + \alpha_{n2}\dot{u}_2 + \gamma_{n1}u_1^3 + \gamma_{n2}u_1^2 u_2 + \gamma_{n3}u_1 u_2^2 + \gamma_{n4}u_2^3)$$
$$= 2f_{n0} + 2\varepsilon f_{n1}\cos(\Omega_1 t - \theta_{n1}) + 2\varepsilon f_{n2}\cos(\Omega_2 t - \theta_{n2}) \tag{1}$$

with $n = 1, 2$ and $|\varepsilon| \ll 1$. Besides the linear terms, these equations include weak cubic non-linearities in the restoring forces. In addition, the external forcing includes constant and harmonic components. The latter are multiplied by the small parameter ε, because this study will focus on the principal external resonances of the system. Thus, it will be assumed in the following that the forcing frequencies satisfy the resonance conditions

$$\Omega_n = \omega_n + \varepsilon\sigma_n. \tag{2}$$

The classical multiple time scales method is then applied in order to determine approximate solutions of the equations examined with the form

$$u_n(t;\varepsilon) = u_{n0}(\tau_0, \tau_1) + \varepsilon u_{n1}(\tau_0, \tau_1) + O(\varepsilon^2), \tag{3}$$

where $\tau_0 = t$ and $\tau_1 = \varepsilon t$ [4]. Substituting the asymptotic expansion (3) into the equations of motion (1) and collecting the zero and first order terms in ε yields the following linear equations:

$$D_0^2 u_{n0} + \omega_n^2 u_{n0} = 2f_{n0}, \tag{4}$$

$$D_0^2 u_{n1} + \omega_n^2 u_{n1} = 2f_{n1}\cos(\Omega_1\tau_0 - \theta_{n1}) + 2f_{n2}\cos(\Omega_2\tau_0 - \theta_{n2}) - 2D_0 D_1 u_{n0}$$
$$- (\alpha_{n1}D_0 u_{10} + \alpha_{n2}D_0 u_{20} + \gamma_{n1}u_{10}^3 + \gamma_{n2}u_{10}^2 u_{20} + \gamma_{n3}u_{10}u_{20}^2 + \gamma_{n4}u_{20}^3), \tag{5}$$

respectively, with $D_m \equiv \partial/\partial\tau_m$. For analytical convenience, the solution of equation (4) is first expressed in the complex form

$$u_{n0} = [h_n + A_n(\tau_1)e_n] + cc, \tag{6}$$

where *cc* denotes the complex conjugate of the preceding terms, while

$$h_n = f_{n0}/\omega_n^2 \quad \text{and} \quad e_n = \mathrm{e}^{\mathrm{i}\omega_n \tau_0}.$$

Then substitution of u_{n0} from equation (6) into equation (5) leads to the following equation:

$$\begin{aligned} D_0^2 u_{n1} + \omega_n^2 u_{n1} = {} & f_{n1}\,\mathrm{e}^{\mathrm{i}(\sigma_1\tau_1 - \theta_{n1})} e_1 + f_{n2}\,\mathrm{e}^{\mathrm{i}(\sigma_2\tau_1 - \theta_{n2})} e_2 - 2\mathrm{i}\omega_n A_n' e_n - \mathrm{i}\omega_1 \alpha_{n1} A_1 e_1 - \mathrm{i}\omega_2 \alpha_{n2} A_2 e_2 \\ & - \gamma_{n1}[A_1^3 e_1^3 + 6h_1 A_1^2 e_1^2 + 3(A_1^2 \bar{A}_1 + 4h_1^2 A_1) e_1 + 6h_1 A_1 \bar{A}_1 + 4h_1^3] \\ & - \gamma_{n2}[A_1^2 A_2 e_1^2 e_2 + A_1^2 \bar{A}_2 e_1^2 \bar{e}_2 + 2h_2 A_1^2 e_1^2 + 4h_1 A_1 A_2 e_1 e_2 + 4h_1 A_1 \bar{A}_2 e_1 \bar{e}_2 \\ & \quad + 8h_1 h_2 A_1 e_1 + (2A_1 \bar{A}_1 A_2 + 4h_1^2 A_2) e_2 + 2h_2 A_1 \bar{A}_1 + 4h_1^2 h_2] \\ & - \gamma_{n3}[A_2^2 A_1 e_2^2 e_1 + A_2^2 \bar{A}_1 e_2^2 \bar{e}_1 + 2h_1 A_2^2 e_2^2 + 4h_2 A_1 A_2 e_1 e_2 + 4h_2 A_2 \bar{A}_1 e_2 \bar{e}_1 \\ & \quad + 8h_1 h_2 A_2 e_2 + (2A_2 \bar{A}_2 A_1 + 4h_2^2 A_1) e_1 + 2h_1 A_1 \bar{A}_2 + 4h_2^2 h_1] \\ & - \gamma_{n4}[A_2^3 e_2^3 + 6h_2 A_2^2 e_2^2 + 3(A_2^2 \bar{A}_2 + 4h_2^2 A_2) e_2 + 6h_2 A_2 \bar{A}_2 + 4h_2^3] + cc. \end{aligned} \tag{7}$$

By a simple inspection of the right-hand side of the last equation it is clearly seen that the presence of the constant forcing terms f_{n0} (or, equivalently, h_n) affects the terms giving rise to 1 : 1 internal resonance. This resonance is typical and together with the 1 : 3 internal resonances, they are expected to occur to first order in systems with symmetric non-linearities [4–12]. However, the system can also exhibit 1 : 2 internal resonance entirely due to the presence of the constant forcing components. If these components are removed, the 1 : 1 and 1 : 3 internal resonances can still exist while the occurrence of the 1 : 2 internal resonance becomes impossible. These observations are analyzed and discussed further in the following two sections.

3. ANALYSIS OF SYSTEMS WITH NO INTERNAL RESONANCE

For the simplest case, where the system examined exhibits no internal resonance, application of standard procedures in equation (7) yields the following set of solvability conditions:

$$\begin{aligned} \mathrm{i}\omega_1(2A_1' + \alpha_{11}A_1) = {} & f_{11}\,\mathrm{e}^{\mathrm{i}(\sigma_1\tau_1 - \theta_{11})} - 3\gamma_{11}(A_1^2\bar{A}_1 + 4h_1^2 A_1) \\ & - 8\gamma_{12}h_1 h_2 A_1 - \gamma_{13}(2A_1 A_2 \bar{A}_2 + 4h_2^2 A_1), \end{aligned} \tag{8}$$

$$\begin{aligned} \mathrm{i}\omega_2(2A_2' + \alpha_{22}A_2) = {} & f_{22}\,\mathrm{e}^{\mathrm{i}(\sigma_2\tau_1 - \theta_{22})} - 3\gamma_{24}(A_2^2\bar{A}_2 + 4h_2^2 A_2) \\ & - 8\gamma_{23}h_1 h_2 A_2 - \gamma_{22}(2A_1 A_2 \bar{A}_1 + 4h_1^2 A_2). \end{aligned} \tag{9}$$

The overbars indicate complex conjugate quantities, while the primes denote differentiation with respect to the slow time τ_1. As usual, expressing the solution amplitudes in the polar form

$$A_n(\tau_1) = \tfrac{1}{2}\alpha_n(\tau_1)\,\mathrm{e}^{\mathrm{i}\beta_n(\tau_1)}, \tag{10}$$

substituting in the solvability conditions (8), (9) and separating the real from the imaginary parts of the resulting relations, leads to a set of slow-flow equations with the following form:

$$\alpha_1' = -c_1\alpha_1 + f_1 \sin\gamma_1, \qquad \alpha_1\gamma_1' = c_2\alpha_1 - c_3\alpha_1^3 - c_4\alpha_1\alpha_2^2 + f_1\cos\gamma_1, \tag{11, 12}$$

$$\alpha_2' = -e_1\alpha_2 + f_2 \sin\gamma_2, \qquad \alpha_2\gamma_2' = e_2\alpha_2 - e_3\alpha_2^3 - e_4\alpha_2\alpha_1^2 + f_2\cos\gamma_2, \tag{13, 14}$$

where

$$\gamma_n(\tau_1) = \sigma_n \tau_1 - \beta_n(\tau_1) - \theta_{nn} \tag{15}$$

and

$$c_1 = \frac{\alpha_{11}}{2}, \qquad c_2 = \sigma_1 - \frac{1}{\omega_1}(4\gamma_{12}h_1h_2 + 6\gamma_{11}h_1^2 + 2\gamma_{13}h_2^2), \qquad c_3 = \frac{3\gamma_{11}}{8\omega_1}, \qquad c_4 = \frac{\gamma_{13}}{4\omega_1},$$

$$e_1 = \frac{\alpha_{22}}{2}, \qquad e_2 = \sigma_2 - \frac{1}{\omega_2}(4\gamma_{23}h_1h_2 + 6\gamma_{24}h_2^2 + 2\gamma_{22}h_1^2), \qquad e_3 = \frac{3\gamma_{24}}{8\omega_2}, \qquad e_4 = \frac{\gamma_{22}}{4\omega_2},$$

$$f_1 = \frac{f_{11}}{\omega_1}, \qquad f_2 = \frac{f_{22}}{\omega_2}.$$

The system of first order autonomous ordinary differential equations (11)–(14) governs the amplitudes and phases of the approximate solutions expressed by equation (3). Note that if $(\alpha_1, \alpha_2, \gamma_1, \gamma_2)$ is a solution of these equations, then it is easy to verify that

$$(-\alpha_1, \alpha_2, \gamma_1 \pm \pi, \gamma_2), \qquad (\alpha_1, -\alpha_2, \gamma_1, \gamma_2 \pm \pi) \quad \text{and} \quad (-\alpha_1, -\alpha_2, \gamma_1 \pm \pi, \gamma_2 \pm \pi)$$

are also solutions. Moreover, combination of relations (2), (6), (10) and (15) with equation (3) shows that the corresponding solutions of the original equations of motion (1) appear in the form

$$u_n(t) = 2h_n + \alpha_n \cos(\Omega_n \tau_0 - \theta_{nn} - \gamma_n) + O(\varepsilon). \tag{16}$$

The above results demonstrate that the constant forcing terms affect the system dynamics only through the terms c_2 and e_2. Also, coupling between the subset of equations (11) and (12) with the subset of equations (13) and (14) is provided through the coefficients γ_{13} and γ_{22} only. If these coefficients are zero, the dynamics are essentially reduced to those exhibited by a single-degree-of-freedom Duffing oscillator (see reference [4]). Similar results are also obtained for the special forcing cases with $f_1 = 0$ or $f_2 = 0$. For instance, in the latter case (or, alternatively, when Ω_2 is not close to ω_2), equation (13) implies that $\alpha_2 \to 0$, provided that the damping parameter α_{22} is positive. Consequently, equation (12) is replaced by

$$\alpha_1 \gamma_1' = c_2\alpha_1 - c_3\alpha_1^3 + f_1 \cos\gamma_1 \tag{17}$$

which together with equation (11) forms a set of slow-flow equations similar to that presented in Appendix A for the single-degree-of-freedom Duffing oscillator subjected to constant and harmonic loading. The main difference is that the term c_2 continues to depend on both h_1 and h_2.

Among the possible solutions of equations (11)–(14), constant solutions are expected to play a dominant role. In order to capture such solutions, all the time derivatives on the left-hand side of these equations are set equal to zero. This leads to a system of four algebraic equations for the unknown amplitudes $(\alpha_{10}, \alpha_{20})$ and phases $(\gamma_{10}, \gamma_{20})$ of these motions. The first two of them are linear in $\sin\gamma_{10}$ and $\cos\gamma_{10}$, with form

$$f_1 \sin\gamma_{10} = c_1\alpha_{10} \quad \text{and} \quad f_1 \cos\gamma_{10} = -c_2\alpha_{10} + c_3\alpha_{10}^3 + c_4\alpha_{10}\alpha_{20}^2. \tag{18}$$

Likewise, the other two equations can be put in the form

$$f_2 \sin\gamma_0 = e_1\alpha_{20} \quad \text{and} \quad f_2\cos\gamma_{20} = -e_2\alpha_{20} + e_3\alpha_{20}^3 + e_4\alpha_{20}\alpha_{10}^2. \tag{19}$$

Squaring and adding both sides of equations (18a) and (18b) results in

$$c_3^2\alpha_{10}^6 + 2c_3c_4\alpha_{10}^4\alpha_{20}^2 + c_4^2\alpha_{10}^2\alpha_{20}^4 - 2c_2c_3\alpha_{10}^4 - 2c_2c_4\alpha_{10}^2\alpha_{20}^2 + (c_1^2 + c_2^2)\alpha_{10}^2 - f_1^2 = 0. \tag{20}$$

Similar manipulation of equations (19a) and (19b) yields

$$e_3^2\alpha_{20}^6 + 2e_3e_4\alpha_{10}^2\alpha_{20}^4 + e_4^2\alpha_{10}^4\alpha_{20}^2 - 2e_2e_3\alpha_{20}^4 - 2e_2e_4\alpha_{10}^2\alpha_{20}^2 + (e_1^2 + e_2^2)\alpha_{20}^2 - f_2^2 = 0. \tag{21}$$

Equations (20) and (21) represent a set of two algebraic equations for the two unknowns $x_1 = \alpha_{10}^2$ and $x_2 = \alpha_{20}^2$. Numerical solution of this system determines the amplitudes of vibration α_{10} and α_{20}. Then, the corresponding phases γ_{10} and γ_{20} are evaluated by simple back substitution in equations (18) and (19). Finally, the stability properties of these motions are determined by applying the classical method of linearization [4].

4. DYNAMICAL SYSTEMS WITH INTERNAL RESONANCE

As usual, the system dynamics becomes more involved when internal resonances are activated. For instances, in the case of a 1:2 internal resonance with

$$\omega_2 = 2\omega_1 + \varepsilon\sigma,$$

the extra terms

$$-4(h_1\gamma_{12} + h_2\gamma_{13})\bar{A}_1A_2\,e^{i\sigma\tau_1} \quad \text{and} \quad -(6h_1\gamma_{21} + 2h_2\gamma_{22})A_1^2\,e^{-i\sigma\tau_1}$$

need to be added on the right-hand side of the solvability conditions (8) and (9) respectively. Obviously, when the mean load is zero both of these terms disappear and the occurrence of the 1:2 internal resonances becomes impossible. On the other hand, this is not the case for the 1:3 internal resonance, which occurs when the frequency condition

$$\omega_2 = 3\omega_1 + \varepsilon\sigma$$

is fulfilled. In this case the extra terms

$$-\gamma_{12}\bar{A}_1^2A_2\,e^{i\sigma\tau_1} \quad \text{and} \quad -\gamma_{21}A_1^3\,e^{-i\sigma\tau_1}$$

need to be included in the solvability conditions (8) and (9). In fact, both of these terms do not depend at all on the constant load components.

The most complicated situation arises when the dynamical system is in a state of a 1:1 internal resonance. This occurs when the linear natural frequencies satisfy the following condition:

$$\omega_2 = \omega_1 + \varepsilon\sigma. \tag{22}$$

The extra terms on the right-hand side of equation (7) that become activated under this internal resonance condition and need to be added in the solvability conditions (8) and (9) are

$$\{f_{12}\,e^{i(\sigma_2\tau_1 - \theta_{12})} - [i\omega_2\alpha_{12} + \gamma_{12}A_1^2 + \gamma_{13}\bar{A}_1A_2e^{i\sigma\tau_1} + \gamma_{12}(2A_1\bar{A}_1 + 4h_1^2) + 8\gamma_{13}h_1h_2 + 3\gamma_{14}(A_2\bar{A}_2 + 4h_2^2)]\,A_2\}\,e^{i\sigma\tau_1}$$

and

$$\{ f_{21}\, e^{i(\sigma_1 \tau_1 - \theta_{21})} - [i\omega_1 \alpha_{21} + \gamma_{22} A_1 \bar{A}_2 e^{-i\sigma\tau_1} + \gamma_{23} A_2^2 + \gamma_{23}(2A_2 \bar{A}_2 + 4h_2^2) + 8\gamma_{22} h_1 h_2 + 3\gamma_{21}(A_1 \bar{A}_1 + 4h_1^2)] A_1 \} e^{i\sigma\tau_1}$$

respectively. Then, applying a procedure similar to that presented in the previous section leads to the following new set of slow-flow equations:

$$\alpha_1' = r_1 \alpha_1 + (r_2 + 3r_3 \alpha_1^2 + r_4 \alpha_2^2)\alpha_2 \sin\gamma + r_5 \alpha_2 \cos\gamma + r_6 \alpha_1 \alpha_2^2 \sin 2\gamma + q_{11} \sin\gamma_1 + q_{12} \sin(\gamma_2 + \gamma + \theta_{22} - \theta_{12}), \tag{23}$$

$$\alpha_1 \gamma_1' = r_7 \alpha_1 + r_8 \alpha_1^3 + 2r_6 \alpha_1 \alpha_2^2 + (r_2 + r_3 \alpha_1^2 + r_4 \alpha_2^2)\alpha_2 \cos\gamma - r_5 \alpha_2 \sin\gamma + r_6 \alpha_1 \alpha_2^2 \cos 2\gamma + q_{11} \cos\gamma_1 + q_{12} \cos(\gamma_2 + \gamma + \theta_{22} - \theta_{12}), \tag{24}$$

$$\alpha_2' = s_1 \alpha_2 + (s_2 + s_3 \alpha_1^2 + 3s_4 \alpha_2^2)\alpha_1 \sin\gamma + s_5 \alpha_1 \cos\gamma + s_6 \alpha_2 \alpha_1^2 \sin 2\gamma + q_{22} \sin\gamma_2 + q_{21} \sin(\gamma_1 - \gamma + \theta_{11} - \theta_{21}), \tag{25}$$

$$\alpha_2 \gamma_2' = s_7 \alpha_2 + s_8 \alpha_2^3 - 2s_6 \alpha_2 \alpha_1^2 - (s_2 + s_3 \alpha_1^2 + s_4 \alpha_2^2)\alpha_1 \cos\gamma + s_5 \alpha_1 \sin\gamma - s_6 \alpha_2 \alpha_1^2 \cos 2\gamma + q_{22} \cos\gamma_2 + q_{21} \cos(\gamma_1 - \gamma + \theta_{11} - \theta_{21}). \tag{26}$$

The constants r_i and s_i are known functions of the system parameters, while the phases γ_n are defined by equation (15) and

$$\gamma = \sigma\tau_1 - \beta_1 + \beta_2.$$

Solution of the set of equations (23)–(26) determines the amplitudes and phases of approximate motions of the original system (1), which are expressed by equation (16) again.

Application of definition (15) in conjunction with the last expression yields the relation

$$\gamma = (\sigma_2 - \sigma_1 + \sigma)\tau_1 + \gamma_1 - \gamma_2 + \theta_{11} - \theta_{22}.$$

Based on this result, it can readily be verified that the new set of slow-flow equations satisfies the same symmetry properties as the set of equations (11)–(14). In addition, the last relation indicates that solutions of the set (23)–(26) with constant phases γ_1 and γ_2 do not actually correspond to constant solutions, since then the phase γ is varying linearly in the slow time τ_1. Moreover, combination of relations (2) and (22) shows that

$$\Omega_2 = \Omega_1 + \varepsilon(\sigma_2 - \sigma_1 + \sigma);$$

namely, the difference between these two frequencies is of order ε, which implies the possibility of strong bearing phenomena. However, in the special case of monofrequency excitation (i.e., when $\Omega_2 = \Omega_1 \equiv \Omega$), which is satisfied when $f_{11} = f_{21} = 0$ or $f_{12} = f_{22} = 0$ in the original system (1), it is easily concluded from the last expressions that

$$\sigma_2 - \sigma_1 + \sigma = 0 \;\Rightarrow\; \gamma = \gamma_1 - \gamma_2 + \theta_{11} - \theta_{22},$$

which converts the set of slow-flow equations (23)–(26) into an autonomous form. Therefore, in this case, *constant solutions* of this set of equations, with $\alpha_1' = \alpha_2' = \gamma_1' = \gamma_2' = 0$ and consequently $\gamma' = 0$, do exist and can be determined by solving the resulting set of algebraic equations. Also, the stability properties of these solutions can be investigated by applying the classical method of linearization [4]. Finally, the same set of equations may also exhibit *periodic solutions*. Determination of such solutions as well as of their stability properties, requires the application of special numerical techniques [14].

5. EXAMPLE MECHANICAL MODEL

The methodology presented in the previous sections is applied to the example mechanical oscillator shown in Figure 1. This oscillator represents a typical half-car model,consisting of a rigid body with mass m and centroidal mass moment of inertia I_G [15]. The car body is supported by two suspensions, modelled by spring–damper elements with linear viscous damping and Duffing-type springs. Consequently, if $z_n(t)$ represents the spring deformation at each suspension ($n = 1, 2$), the corresponding force developed has the form $c_n\dot{z}_n + k_n z_n + \lambda_n z_n^3$. In the cases examined, the excitation arises from harmonic road irregularities with horizontal distribution $s(y) = s_0 \cos(2\pi y/l)$. Therefore, if the horizontal velocity component of the car body is constant and equal to v_0, these irregularities lead to a harmonic base excitation of the vehicle with frequency $\omega = 2\pi v_0/l$. Then, introducing the dimensionless time and displacement co-ordinates of the system with the definitions

$$\tau = \omega_c t \quad \text{and} \quad x_n(\tau) = z_n(t)/z_c,$$

where ω_c and z_c represent a characteristic frequency and length of the system, respectively, its equations of motion can be put into the normalized form

$$\mathbf{M}\ddot{\mathbf{x}} + \mathbf{K}\mathbf{x} + \hat{\boldsymbol{\eta}}(\mathbf{x}, \dot{\mathbf{x}}) = \hat{\mathbf{f}}(\tau) \tag{27}$$

with

$$\mathbf{x} = \begin{pmatrix} x_1 \\ x_2 \end{pmatrix}, \qquad \mathbf{M} = \begin{bmatrix} 1 & \beta \\ -1 & 1 \end{bmatrix}, \qquad \mathbf{K} = \begin{bmatrix} 1 & \kappa \\ -1/\mu & \kappa/\beta\mu \end{bmatrix}, \qquad \hat{\mathbf{f}}(\tau) = -\hat{g}\begin{pmatrix} 1 \\ 0 \end{pmatrix}$$
$$+ \hat{s}\begin{pmatrix} \hat{f}_1 \cos(\Omega\tau - \varphi_1) \\ \hat{f}_2 \cos(\Omega\tau - \varphi_2) \end{pmatrix}, \qquad \hat{\boldsymbol{\eta}}(\mathbf{x}, \dot{\mathbf{x}}) = 2\hat{\zeta}\begin{pmatrix} \dot{x}_1 + c\dot{x}_2 \\ (c\dot{x}_2 - \beta\dot{x}_1)/\beta\mu \end{pmatrix} + \varepsilon\begin{pmatrix} x_1^3 + \lambda x_2^3 \\ (\lambda x_2^3 - \beta x_1^3)/\beta\mu \end{pmatrix}.$$

The parameters appearing in the latter expressions are functions of the following independent dimensionless parameters

$$\Omega = \frac{\omega}{\omega_c}, \qquad \zeta_1 = \frac{c_1}{2\sqrt{k_1 m}}, \qquad \mu = \frac{I_G}{mab}, \qquad \nu = \frac{a}{l}, \qquad \beta = \frac{a}{b}, \qquad \hat{s} = \frac{s_0}{z_c},$$
$$\varepsilon = \frac{\lambda_1 z_c^2}{k_1}, \qquad \kappa = \frac{k_2}{k_1}, \qquad \lambda = \frac{\lambda_2}{\lambda_1}, \qquad c = \frac{c_2}{c_1}, \qquad \hat{g} = \frac{mg}{k_1 z_c}.$$

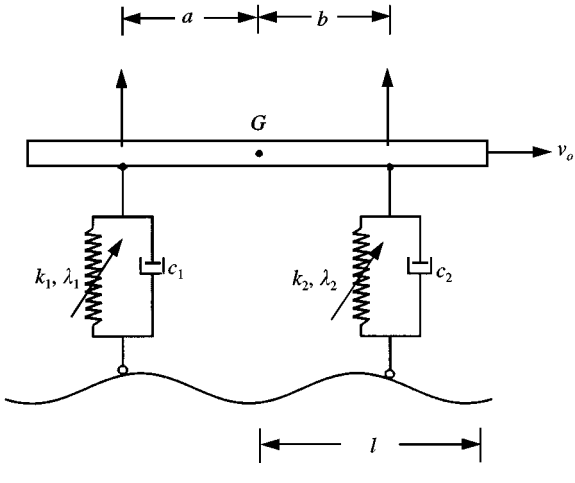

Figure 1. Mechanical model.

For instance, $\hat{\zeta} = \zeta_1 \sqrt{1+\beta}$ and $\omega_c = \sqrt{(1+\beta)\, k_1/m}$. In addition, one of the forcing parameters $\hat{s}$ and $\hat{g}$ may be eliminated by a proper choice of the characteristic length z_c.

Next, a suitable methodology is applied, bringing the equations of motion (27) into the canonical form (1). This is accomplished by solving the eigenvalue problems

$$(\mathbf{K} - \omega_n^2 \mathbf{M})\, \boldsymbol{\phi}_n = \mathbf{0}, \qquad (\mathbf{K}^{\mathrm{T}} - \omega_n^2 \mathbf{M}^{\mathrm{T}})\, \boldsymbol{\psi}_n = \mathbf{0}$$

and forming the modal matrices $\boldsymbol{\Phi} = [\boldsymbol{\phi}_1\ \boldsymbol{\phi}_2]$ and $\boldsymbol{\Psi} = [\boldsymbol{\psi}_1\ \boldsymbol{\psi}_2]$ of the right and left eigenvectors, respectively, so that they satisfy the following bi-orthogonality conditions

$$\boldsymbol{\Psi}^{\mathrm{T}} \mathbf{M} \boldsymbol{\Phi} = \mathbf{I} = \begin{bmatrix} 1 & 0 \\ 0 & 1 \end{bmatrix} \quad \text{and} \quad \boldsymbol{\Psi}^{\mathrm{T}} \mathbf{K} \boldsymbol{\Phi} = \boldsymbol{\Lambda} \equiv \begin{bmatrix} \omega_1^2 & 0 \\ 0 & \omega_2^2 \end{bmatrix}. \tag{28}$$

Then employing the co-ordinate transformation

$$\mathbf{x} = \boldsymbol{\Phi} \mathbf{u}, \tag{29}$$

substituting in equation (27), premultiplying both sides of the resulting equation with $\boldsymbol{\Psi}^{\mathrm{T}}$, setting

$$\hat{\zeta} = \varepsilon \zeta$$

and employing the bi-orthogonality relations (28), leads to

$$\ddot{\mathbf{u}} + \boldsymbol{\Lambda} \mathbf{u} + \varepsilon \boldsymbol{\eta}(\mathbf{u}, \dot{\mathbf{u}}) = \mathbf{f}(\tau) \tag{30}$$

with

$$\varepsilon \boldsymbol{\eta}(\mathbf{u}, \dot{\mathbf{u}}) = \boldsymbol{\Psi}^{\mathrm{T}} \hat{\boldsymbol{\eta}}(\boldsymbol{\Phi}\mathbf{u}, \boldsymbol{\Phi}\dot{\mathbf{u}}) \quad \text{and} \quad \mathbf{f}(\tau) = \boldsymbol{\Psi}^{\mathrm{T}} \hat{\mathbf{f}}(\tau) = 2\mathbf{f}_0 + \mathbf{f}_1(\tau).$$

In particular, the time-dependent part of the excitation vector can be set in the form

$$\mathbf{f}_1(\tau) = 2\varepsilon \begin{pmatrix} f_{11} \cos(\Omega\tau - \theta_{11}) \\ f_{21} \cos(\Omega\tau - \theta_{21}) \end{pmatrix}$$

which eventually brings equation (30) into the form of equation (1) with $\mathbf{f}_2(\tau) = \mathbf{0}$. This corresponds to monofrequency excitation with $\Omega_2 = \Omega_1 \equiv \Omega$. Therefore, based on equations (16) and (29), it is concluded that a constant solution of equations (23)–(26) corresponds to a periodic motion of the dynamical system expressed by equation (27). On the other hand, a periodic solution of the same set of equations represents a quasiperiodic motion of the mechanical system examined.

6. RESPONSE DIAGRAMS

This section presents numerical results obtained for the example mechanical system introduced in the previous section. As it is clear from the form of the mass and stiffness matrix of this system, its linear natural frequencies are functions of the parameters β, κ and μ only. Initially, it is assumed that the system is close to conditions of 1 : 1 internal resonance. Figure 2 shows curves on the (μ, κ) plane, determined for $\beta = 1{\cdot}31$ and several levels of detuning $\varepsilon\sigma$, so that frequency relation (22) is fulfilled. From these results, it is easily observed that for given β, μ and natural frequency detuning $\varepsilon\sigma$, this condition is satisifed for two different values of the stiffness ratio parameter κ, except for the case of the pure 1 : 1 internal resonance.

Next, a series of frequency-response diagrams is presented, after solving the averaged equations (23)–(26) for constant and periodic solutions by employing AUTO [14]. First, the

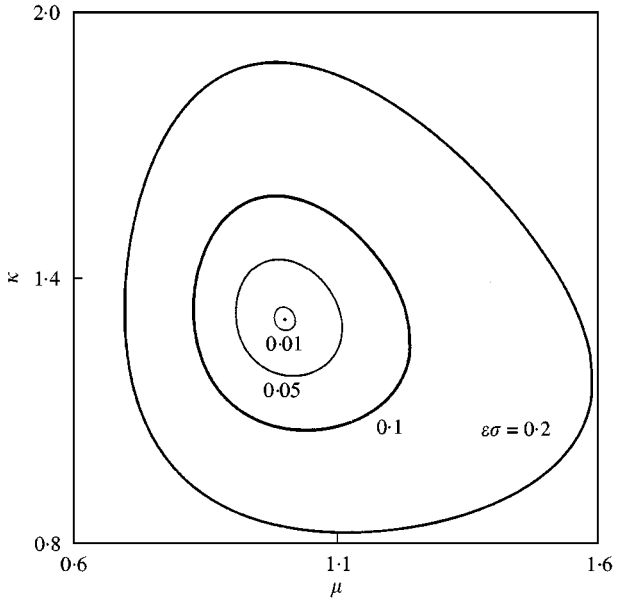

Figure 2. Curves on the (μ, κ) plane obtained for $\beta = 1{\cdot}31$ and several frequency detuning levels.

diagrams of Figure 3 illustrate the effect of the damping parameter ζ on the system response. These diagrams were obtained for different values of the damping parameter ζ, while the other technical parameters were held constant. More specifically, the following set of parameters was chosen: $\varepsilon = 0{\cdot}01$, $\lambda = 1$, $\mu = 1{\cdot}1$, $\nu = 0{\cdot}048$, $\hat{g} = 2$ and $\hat{s} = 0{\cdot}1$. In addition, the value of the stiffness ratio parameter κ was chosen so that $\sigma = 5$, while the damping ratio parameter was selected so that $c = \sqrt{\beta\kappa\mu}$. In all cases, the broken lines represent branches of unstable solutions, while the branches of periodic solutions are represented by thicker lines.

The numerical results of Figure 3 demonstrate that for relatively large values of ζ, the response amplitudes are quite small. As a consequence, the effect of the non-linearities considered is not important. However, by decreasing the value of ζ, the gradual increase in the solution amplitudes makes the presence of the model non-linearities progressively more pronounced. This is marked by the classical bending of the response diagrams and the appearance of coexisting constant and periodic solutions. In particular, Figure 3(d) shows details in the forcing frequency range of Figure 3(c), where the branch of stable periodic solutions terminates.

Qualitatively similar response diagrams were obtained by varying the other system parameters. For instance, the diagrams of Figure 4 show the effect of the constant loading parameter, expressed by $\hat{g}$. These diagrams were determined after setting $\zeta = 0{\cdot}004$, for $\hat{g} = 0$ (corresponding to the symmetric loading case) and $\hat{g} = 8$. Note that Figure 3(b) is also part of the same sequence of diagrams, with $\hat{g} = 2$.

Finally, among all the parameters, the inertia parameter μ was found to have a dominant effect in the natural frequency detuning of the system.This is illustrated by Figure 5, which shows response diagrams obtained for $\mu = 1{\cdot}1$ and 3, leading to values of the detuning parameter σ equal to 5 and 42·68 respectively. Here, the thicker lines represent constant solutions determined by solving the set of slow-flow equations (11)–(14), which were developed for the case of no internal resonance. Direct comparison of the results indicates

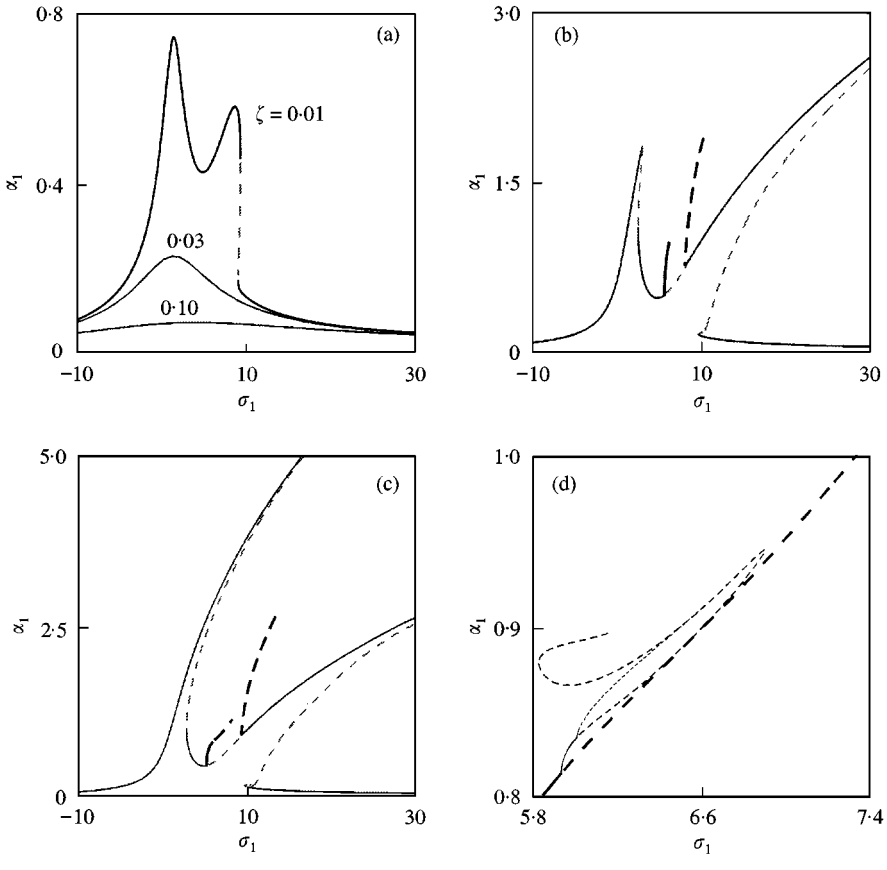

Figure 3. Frequency-response diagram of amplitude α_1 for: (a) $\zeta_1 = 0{\cdot}1$, 0·03 and 0·01, (b) $\zeta_1 = 0{\cdot}004$, (c) and (d) $\zeta_1 = 0{\cdot}0015$.

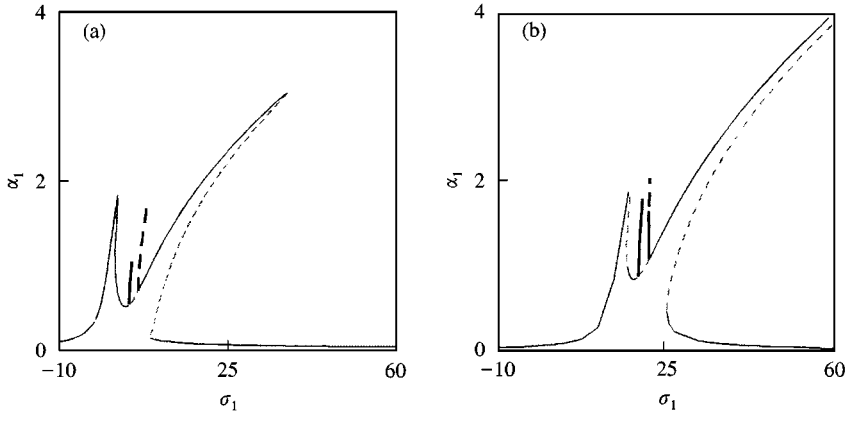

Figure 4. Frequency-response diagram of amplitude α_1 for: (a) $\hat{g} = 0$ and (b) $\hat{g} = 8$.

that the larger the detuning parameter σ, the more accurate the predictions of the latter set of equations become, as expected.

At all points of the frequency-response diagrams presented in this section where vertical tangency occurs, branches of constant solutions are generated or disappear through

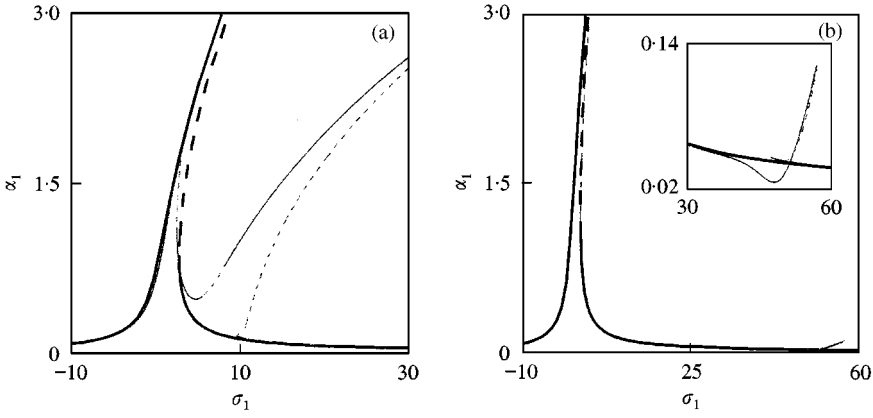

Figure 5. Frequency-response diagram of amplitude α_1 for: (a) $\sigma = 5$ and (b) $\sigma = 42{\cdot}68$.

saddle-node bifurcations. On the other hand, branches of periodic solutions originate from points corresponding to parameter combinations leading to a Hopf bifurcation of a constant solution [13]. If the parameters are such that secondary bifurcations can occur after the original Hopf bifurcation, the system may exhibit complicated and exotic dynamics. The following section presents results for such a case.

7. DIRECT INTEGRATION OF SLOW-FLOW EQUATIONS

This section presents results obtained by direct integration of the slow-flow equations (23)–(26) and in particular for the parameters corresponding to the response diagram of Figure 3(d). More specifically, Figure 6 shows the projection of the system trajectories on the (α_1, α_2) plane for several values of the forcing frequency near the Hopf bifurcation at about $\sigma_1 = 5{\cdot}17$. First, the stable constant solution captured at $\sigma_1 = 5{\cdot}16$ (represented by a dot) gives way to periodic response after the Hopf bifurcation (represented by closed curves), as shown in Figure 6(a). With a further increase in the value of σ_1, this response undergoes a sequence of period doublings (Figures 6(b) and 6(c)), leading eventually to chaotic motion (Figure 6(d)). Moreover, at some point, a sudden explosion of the original attractor occurs, leading to a new and considerably bigger chaotic attractor (Figure 6(e)).

Due to the symmetry properties of the set of equations examined, for every solution appearing in the first quadrant of the (α_1, α_2) plane, there exist three more conjugate solutions in the remaining three quadrants of the plane, resulting from proper reflections on the α_1 and α_2 axes. In fact, the attractors of such solutions may sometimes collide with each other, leading to trajectories visiting two quadrants of the (α_1, α_2) plane (Figure 6(f)). This was followed by forcing frequency intervals where the trajectories return entirely to a single quadrant again (Figure 6(g)). This interchange was seen to take place repeatedly in the present system by varying σ_1. Actually, for some values of σ_1, the trajectories were found to visit all four quadrants of the (α_1, α_2) plane, as illustrated in Figure 6(h).

Similar phenomena were observed in some other recent studies, where they were related to satisfaction of Silnikov conditions by the dynamical systems examined [12, 16, 17]. Moreover, it was first shown in reference [12] that these phenomena were associated with certain changes in the phases of vibration. Similar and even more complicated phases response was also detected in the present investigation. For instance, Figure 7 shows the

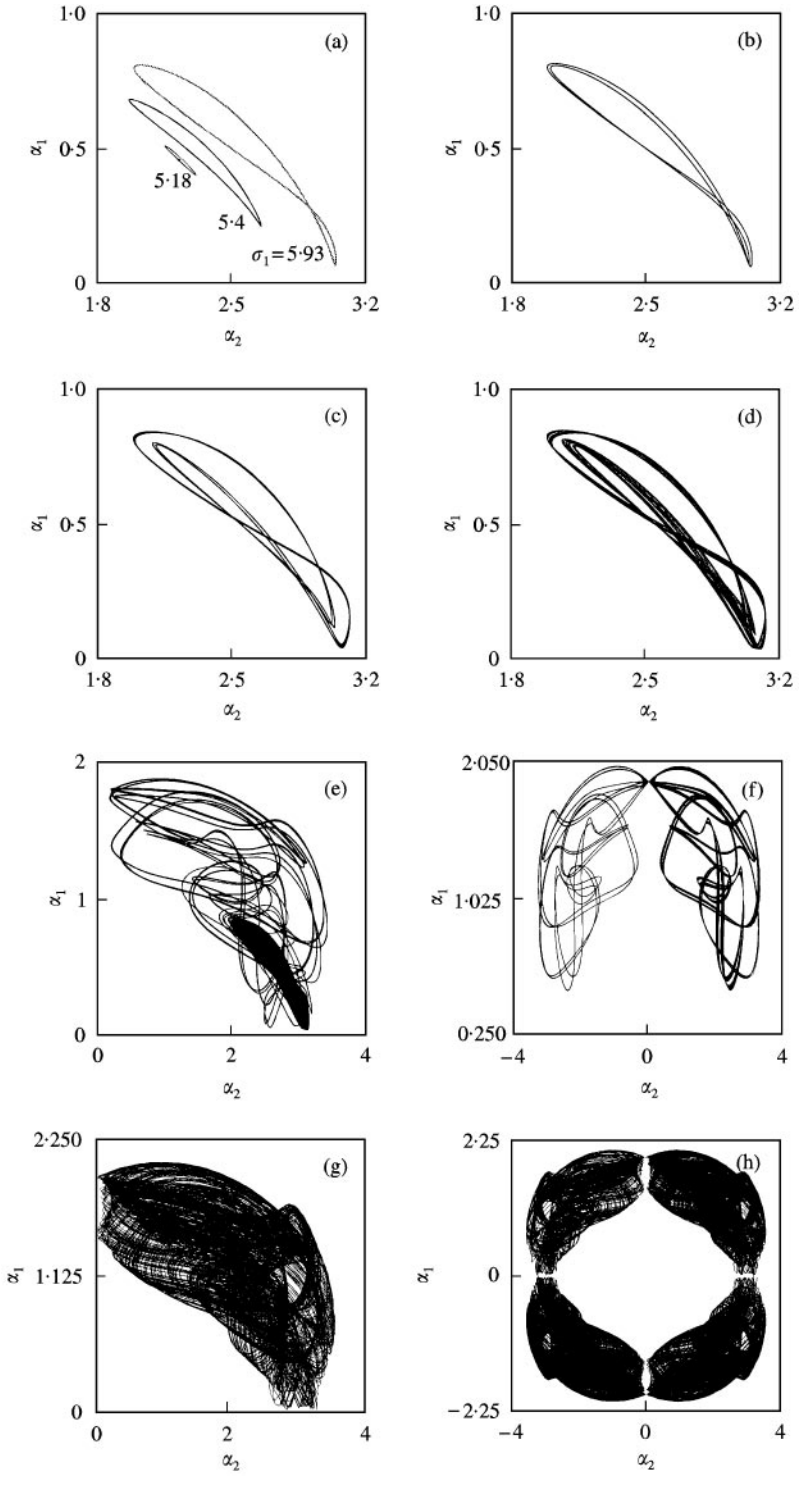

Figure 6. Trajectories on the (α_1, α_2) plane at: (a) $\sigma_1 = 5{\cdot}16$, $5{\cdot}18$, $5{\cdot}4$ and $5{\cdot}93$, (b) $\sigma_1 = 5{\cdot}935$, (c) $\sigma_1 = 6{\cdot}01$, (d) $\sigma_1 = 6{\cdot}027$, (e) $\sigma_1 = 6{\cdot}036418$, (f) $\sigma_1 = 6{\cdot}2196$, (g) $\sigma_1 = 6{\cdot}3$ and (h) $\sigma_1 = 6{\cdot}34$.

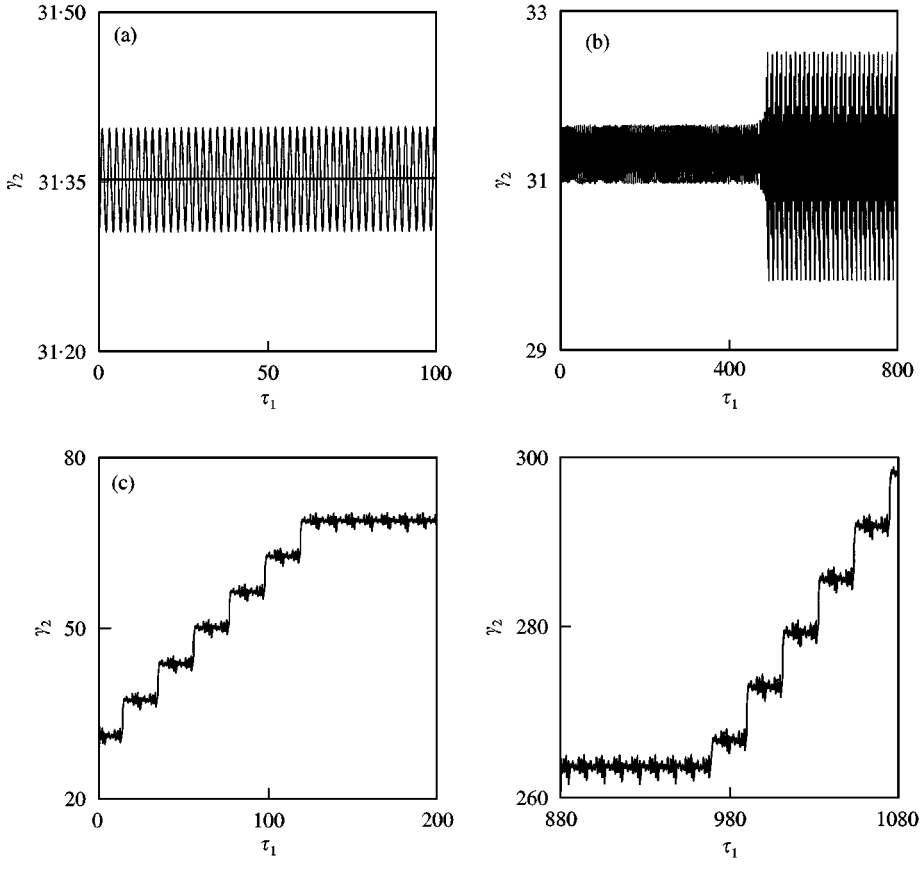

Figure 7. Time histories of phase γ_2 at: (a) $\sigma_1 = 5{\cdot}18$, (b) $\sigma_1 = 6{\cdot}036418$, (c) $\sigma_1 = 6{\cdot}219445$ and (d) $\sigma_1 = 6{\cdot}2196$.

characteristic changes observed in the time history of phase γ_2, for the parameters and the forcing frequency interval of Figure 6. First, Figure 7(a) shows the time history at $\sigma_1 = 5{\cdot}16$ and $5{\cdot}18$, indicating the change from phase locked (constant) to entrained (periodic) response,. occurring after the Hopf bifurcation [18]. Likewise, Figure 7(b) presents the changes observed in the history of γ_2 at the attractor explosion presented in Figure 6(e). After this explosion, the phase γ_2 may occasionally develop a 2π drift (Figure 7(c)). In addition, at the time instances where the trajectory moves to a different quadrant, a phase drift with magnitude π occurs (Figure 7(d)). In accordance with the results presented in reference [12], this is due to the symmetry property

$$(\alpha_1, \alpha_2, \gamma_1, \gamma_2) \rightarrow (\alpha_1, -\alpha_2, \gamma_1, \gamma_2 + \pi)$$

exhibited by the system examined.

For $\sigma_1 > 6{\cdot}2196$, phase γ_2 appears to develop a continuous drift. However, within some relatively short forcing frequency intervals, this was found to occasionally be interrupted by intervals where the drift stops. For example, Figure 8 shows the response obtained at $\sigma_1 = 6{\cdot}34161$. At some point, the original chaotic attractor (Figure 8(a)) is replaced quite rapidly by a similar attractor with simpler from (Figure 8(b)). The time history of amplitude α_2 within the time interval needed for the development of these trajectories is shown in

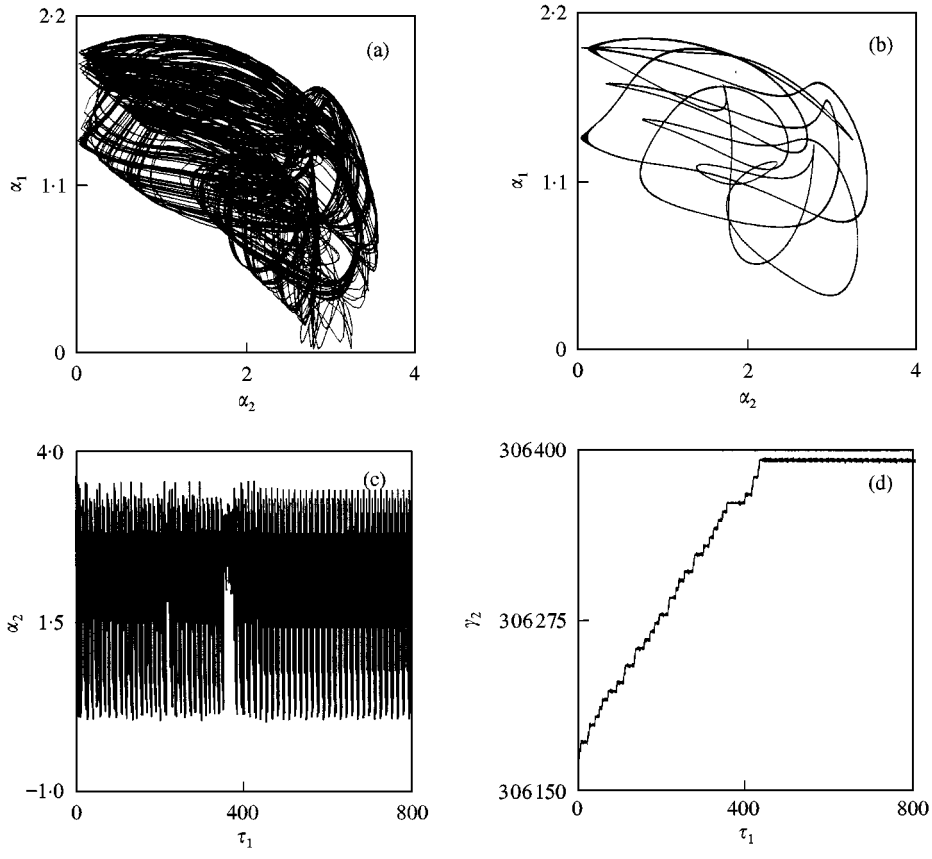

Figure 8. Boundary crisis of $\sigma_1 = 6{\cdot}34161$: (a) trajectories of the original attractor on the (α_1, α_2) plane, (b) trajectories of the new attractor on the (α_1, α_2) plane, (c) time history of amplitude α_2 and (d) time history of phase γ_2.

Figure 8(c), while the corresponding time history of phase γ_2 is shown in Figure 8(d), demonstrating the drift interruption. With a slight increase in the forcing frequency, the attractor shape quickly regains its original complexity and phase γ_2 exhibits a gradual transition towards full drift again.

Finally, it should be noted that phase γ_1 exhibits a different and simpler route to full drift; namely, near the Hopf bifurcation at $\sigma_1 = 5{\cdot}17$, this phase follows exactly the same transition pattern from locking to entrainment as phase γ_2. However, beginning with the explosion of the attractor shown in Figure 6(e), the time history of phase γ_1 was found to develop a permanent drift (Figure 9(a)), which persisted for all the subsequent time and values of the forcing frequency. For completeness in the presentation, the time history of amplitude α_1, corresponding to the same time interval, is also shown in Figure 9(b).

8. SYNOPSIS AND CONCLUSIONS

An analysis method has been developed for investigating the effect of a load-induced asymmetry in the response of a general class of two-degree-of-freedom dynamical systems, with symmetric non-linearities in the restoring forces. The non-linearities are weak and this

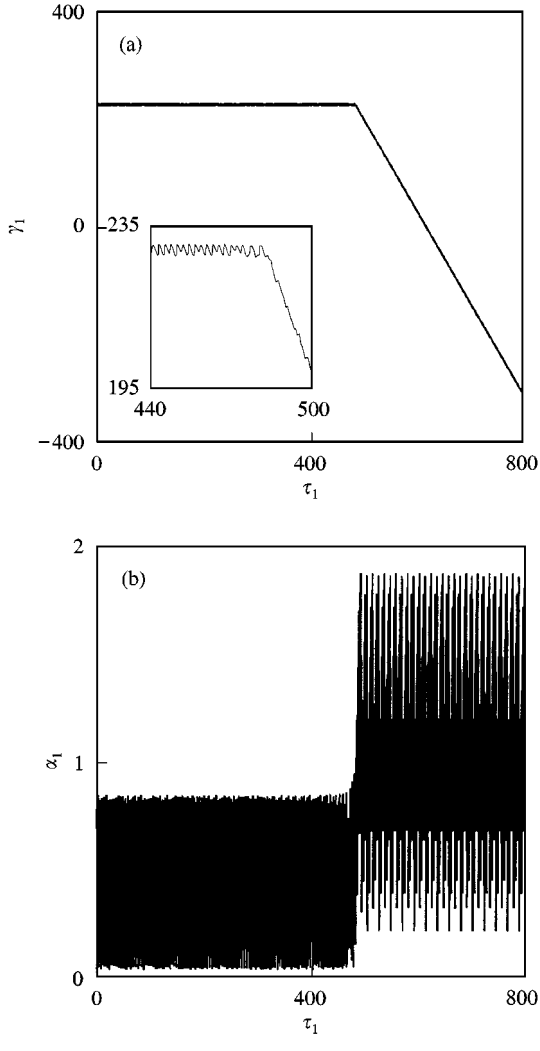

Figure 9. Time history of: (a) phase γ_1 and (b) amplitude α_1, at $\sigma_1 = 6{\cdot}036418$.

permits determination of approximate analytical solutions by applying appropriate singular perturbation procedures. It was first shown that the presence of a constant load component affects the classical 1 : 1 and 1 : 3 internal resonances but, more importantly, it makes possible the appearance of 1 : 2 internal resonances to first order. Sets of slow-flow equations were then derived, governing the amplitudes and phases of approximate motions occurring in cases without internal resonance and for systems near conditions of 1 : 1 internal resonance.

The analysis was subsequently applied to an example mechanical system, for which representative numerical results were obtained. These results were first presented in the form of frequency-response diagrams and demonstrated the effect of selected system parameters on its dynamics. In particular, a decrease in the damping level was found to lead to a more pronounced effect of the non-linearities. This was manifested by the classical bending of the response curves, resulting in a coexistence of stable and unstable branches of

constant and periodic solutions. Finally, these results were complemented with results obtained by direct integration of the slow-flow equations, revealing the existence of a period-doubling sequence of periodic motions, leading eventually to quasiperiodic and chaotic solutions. Apart from the classically observed phenomena, these results illustrate a new transition scenario from phase-locked to phase-entrained and finally drift response.

ACKNOWLEDGMENTS

This work was partially supported by a grant from the General Secretariat of Research and Technology, Greek Ministry of Development, through the Greek–Hungarian Research and Technology Program.

REFERENCES

1. P. R. SETHNA and A. K. BAJAJ 1978 *Journal of Applied Mechanics* **45**, 895–902. Bifurcations in dynamical systems with internal resonance.
2. A. G. HADDOW, A. D. S. BARR and D. T. MOOK 1984 *Journal of Sound and Vibration* **97**, 451–473. Theoretical and experimental study of modal interactions in a two-degree-of-freedom structure.
3. B. BALACHANDRAN and A. H. NAYFEH 1991 *Nonlinear Dynamics* **2**, 77–117. Observations of modal interactions in resonantly forced beam-mass structures.
4. A. H. NAYFEH and D. T. MOOK 1979 *Nonlinear Oscillations*. New York: Wiley-Interscience.
5. A. H. NAYFEH and B. BALACHANDRAN 1989 *Applied Mechanics Reviews* **42**, S175–201. Modal interactions in dynamical and structural systems
6. J. C. CHEN and C. D. BABCOCK 1975 *American Institute of Aeronautis and Astronautics Journal* **13**, 868–876. Nonlinear vibration of cylindrical shells.
7. J. W. MILES 1984 *Journal of Fluid Mechanics* **149**, 15–31. Resonantly forced surface waves in a circular cylinder.
8. J. M. JOHNSON and A. K. BAJAJ 1989 *Journal of Sound and Vibration* **128**, 87–107. Amplitude modulated and chaotic dynamics in resonant motion of strings.
9. A. F. VAKAKIS 1992 *Acta Mechanica* **95**, 197–226. Dynamics of a nonlinear periodic structure with cyclic symmetry.
10. W.-M. TIEN, N. S. NAMACHCHIVAYA and N. MALHOTRA 1994 *International Journal of Non-Linear Mechanics* **29**, 367–386. Non-linear dynamics of a shallow arch under periodic excitation — II. 1 : 1 Internal resonance.
11. S. NATSIAVAS and P. TRATSKAS 1996 *Journal of Sound and Vibration* **194**, 173–185. On vibration isolation of mechanical systems with nonlinear foundations.
12. S. NATSIAVAS and P. METALLIDIS 1997 *Journal of Sound Vibration* **208**, 211–224. External primary resonance of self-excited oscillators with 1 : 3 internal resonance.
13. S. WIGGINS 1990 *Introduction to Applied Nonlinear Dynamical Systems and Chaos*. New York: Springer-Verlag.
14. E. DOEDEL 1986 *AUTO Software for Continuation and Bifurcation Problems in Ordinary Differential Equations*. Pasadena. CA: California Institute of Technology.
15. T. D. GILLESPIE 1992 *Fundamentals of Vehicle Dynamics*. Warrendale, PA: Society of Automotive Engineers.
16. S. SAMARANAYAKE, A. K. BAJAJ and O. D. I. NWOKAH 1995 *Acta Mechanica* **109**, 101–125. Amplitude modulated dynamics and bifurcations in the resonant response of a structure with cyclic symmetry.
17. S. NATSIAVAS and S. THEODOSSIADES 1998 *International Journal of Non-linear Mechanics* **33**, 843–845. Regular and chaotic forced vibration of thin rotating rings.
18. T. CHAKRABORTY and R. H. RAND 1988 *International Journal of Non-Linear Mechanics* **23**, 369–376. The transition from phase locking to drift in a system of two weakly coupled van der Pol oscillators.

APPENDIX A: DUFFING OSCILLATOR UNDER PERIODIC FORCING

Application of the multiple time scales method to a weakly non-linear Duffing oscillator with equation of motion

$$\ddot{u} + \omega_0^2 u + \varepsilon(2\mu\dot{u} + \beta u^3) = 2f_0 + 2\varepsilon f_1 \cos \Omega t$$

for $|\varepsilon| \ll 1$ and under conditions of primary external resonance, expressed by the frequency relation

$$\Omega = \omega_0 + \varepsilon\sigma$$

shows that it accepts approximate analytical solution of the form

$$u(t) = 2h + \alpha \cos(\Omega\tau_0 - \gamma) + O(\varepsilon).$$

The amplitude and phase of the harmonic response component satisfy the slow-flow equations

$$\alpha' = -\mu\alpha + \hat{f} \sin \gamma, \qquad \alpha\gamma' = \hat{\sigma}\alpha - \hat{c}\alpha^3 + \hat{f} \cos \gamma,$$

where

$$\hat{\sigma} = \sigma - \frac{6\beta h^2}{\omega_0}, \qquad \hat{c} = \frac{3\beta}{8\omega_0}, \qquad \hat{f} = \frac{f_1}{\omega_0}, \qquad h = \frac{f_0}{\omega_0^2}.$$

These results are almost identical with those obtained for the case of harmonic external excitation alone. The only effect of the constant forcing component is felt through the modification of the detuning parameter $\hat{\sigma}$.